LUND UNIVERSITY
Faculty of Science

Studies of Dark Matter Signals at the LHC

Martin Angelsmark

Thesis submitted for the degree of Bachelor of Science
Project duration: 5 months

Supervised by Caterina Doglioni, William Kalderon

Department of Physics
Division of Particle Physics
May, 2017

Abstract

Standard matter, the matter that we can see, only make up about 6% of the universe. Astronomical observations have found that there exist other matter, which is non-luminous, called dark matter. This matter can interact gravitationally with standard matter [1], but it is unknown if it can interact weakly with the help of some other force as well. If such interactions were possible, events between dark matter and standard matter could be created in a particle accelerator.

This thesis has studied simulations of dark matter events possible in the ATLAS detector [2] at the Large Hadron Collider [3]. Our theoretical models include a mediator, a particle carrying the force between interacting particles, that can interact with both the standard matter particles called quarks and dark matter. When two quarks collide, it is now possible for them to decay into the mediator particle. This mediator can decay back into two quarks, which will be detected as jets. The invariant mass of the two jets will be equal to the mass of the mediator. Such events, called *di-jet*, have been examined in this thesis.

The simulated events were generated in MadGraph5 [4]. The simulations are divided into different levels. At parton level only the interaction between quarks is considered. At particle level the creation of jets is simulated and will introduce a smearing to the energy values. The last level includes how the particles interact with the detector, which will add further smearing. At the end the measured energies will have a certain resolution caused by the smearing. This thesis compares the resolution at particle level and detector level. Furthermore, the energies at particle level were smeared using a simple formula to approximate the effects of the detector. These smeared values were compared to the values at detector level and seem to suggest that it is a good approximation. The detector level is more involved than particle level and parameterization of the detector resolution will thus save time for future *di-jet event* simulations.

Abbreviations

DM	Dark Matter
LHC	Large Hadron Collider
MC	Monte Carlo
SM	Standard Model
LO	Leading Order
NLO	Next to Leading Order
EM	Electromagnetic
QCD	Quantum Chromo Dynamics
CMB	Cosmic Microwave Background
WIMP	Weakly Interactig Massive Particle
FWHM	Full Width at Half Maximum
FSR	Final State Radiation
ISR	Initial State Radiation

Acknowledgments

I want to thank my supervisors Caterina and Will for all of the help. Enormous thanks to my main supervisor Caterina for taking time of her busy schedule to answer my questions and help me in the writing process. Also thanks to Will, especially for providing me with all the detector level generations I needed. Working on this project has been a wonderful experience and it further convinced me to continue within the field of particle physics.

During my education I have had huge support behind me. Thus I want to thank all my classmates and dear friends, my family and my beloved partner Elin Johansson Hoff. Thank you, your support means everything.

Contents

1 Introduction

Over the course of the 20th century, a number of observations showed a lack of luminous matter in the universe. This missing matter has been called dark matter (DM). Explaining its nature is the focus of many theoretical efforts and experimental searches. There is compelling evidence for dark matter in astronomical observations but none in particle physics [1]. If a dark matter particle would be observed in a detector it would be possible to investigate its properties. To help in dark matter searches at the Large Hadron Collider (LHC) [3] *di-jet* dark matter events have been generated using the Monte Carlo (MC) generator MadGraph5 [4]. The standard model (SM) describes the smallest known building blocks of matter [5]. When two SM particles collide and decay into the dark matter mediator (a mediator carries the force between particles), the mediator can then decay back into SM or DM. If it decays into the SM particles quarks, these will form two jets, which are collimated sprays of particles, that can be detected as a *di-jet event* [6].

The simulated events were generated at detector level that includes the effects of the ATLAS detector [2] and TRUTH level which does not include these effects. A smearing on the energies was applied to the TRUTH level in order to approximate the effects of the detector and was compared to the detector level. If the TRUTH level has a similar distribution to the detector level, future simulations will only need to generate at TRUTH level. This will save time since TRUTH level generations are less involved.

This thesis will start by introducing the standard model in section 2.1. It will continue to describe the detection and theoretical models of dark matter in section 2.2 Dark Matter. Section 2 Theory also includes section 2.4 about detection at colliders, section 2.5 about MC generators and section 2.6 about summary plots. Section 3 Method describes the models used and how they were compared. The results are presented and discussed in sections 4 Results. Section 5 Outlook talks about the implications of the results and future research.

2 Theory

2.1 The Standard Model

2.1.1 Elementary particles

The Standard Model is a theory that tries to explain the smallest known building blocks and the forces between them. In the SM there are both particles that make up matter as we know it and particles that carry the forces between them. These particles are thought to be pointlike, which means that they have no substructure, and are thus called elementary particles. This statement is valid so far at the current energy scales that the particles can be probed with. A substructure might be seen when higher energy scales has been achieved in future accelerators. All of the particles are listed in figure 1 and

are divided into fermions with spin-half and bosons with integer spin. The fermions are categorized into leptons who only take part in electromagnetic and weak interaction and quarks which have a color charge and thus take part in the strong interactions as well. For both leptons and quarks there exist three generations of particles. The first generation consist of stable particles, and there is an increase in mass for increasing generation. For the bosons there exist four gauge bosons that are force carriers of the fundamental forces except gravity – the force carriers are also called mediators – and one scalar boson, which is the Higgs and gives mass to particles.

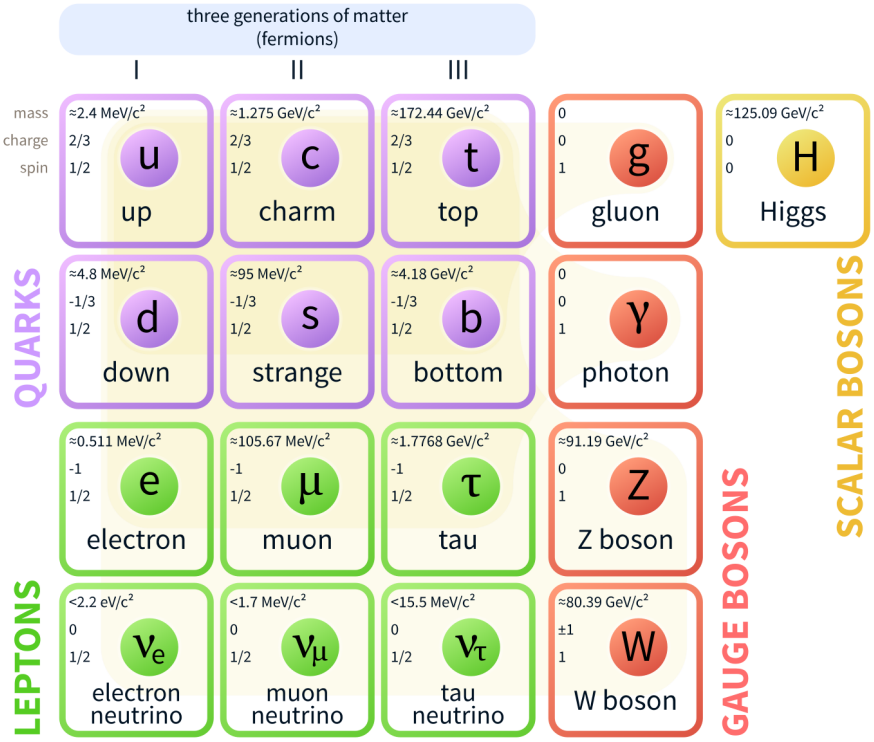

Figure 1: Figure displaying all elementary particles included in the SM [7].

The strong interaction mediator particle is the gluon and the electromagnetic (EM) interaction is mediated by the photon. The weak interaction has three mediators, which are the W^+, W^- and Z bosons [8].

2.1.2 Cross Section

The cross section for an interaction is proportional to the absolute value of the matrix element M_{fi} squared. The expression for an interaction $a + b \rightarrow c + d$ is:

$$\frac{d\sigma}{d\Omega^*} = \frac{1}{64\pi^2 s}\frac{p_f^*}{p_i^*}|M_{fi}|^2 \tag{1}$$

calculated in the center-of-mass frame. Here, Ω^* is the solid angle and s is the center-of-mass energy squared. Also, $p_f^* = p_c = -p_d$ is the final state momentum and $p_i^* = p_a = -p_b$ is the initial state momentum, where p_k $(k = a, b, c, d)$ is the momentum for particle k.

M_{fi} can be found using Feynman rules, a set of rules that can be applied to any Feynman diagrams. In an interaction of leading order (LO) between two particles a and b there will be two vertexes and a mediator. An elastic interaction is seen in figure 2. The vertexes represent the factor coming from particle a or b emitting (or absorbing) the mediator. This factor will be proportional to the coupling constant α, which determines how much the mediator couples to the particles included in the interaction, of the interaction. There will also be a propagator term q contributed by the mediator which is proportional to the four-momentum and mass of the mediator. These three factors multiplied yield $-iM_{fi}$ which means that the probability for a LO interaction to happen is proportional to the coupling constant squared and the mass of the mediator. For next-to-leading order (NLO) or higher there will be additional vertexes, in form of initial- or final-state radiation or loops, that decreases the probability of the event to happen [8].

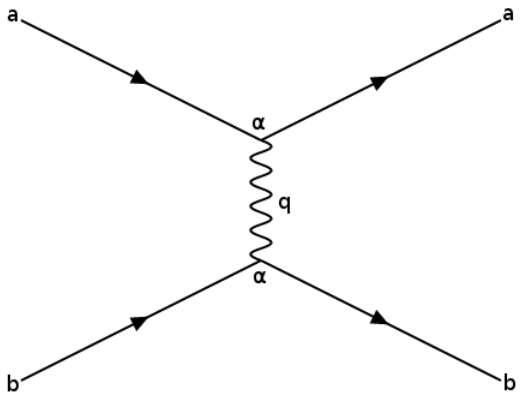

Figure 2: A Feynman diagram of an elastic interaction between particle a and b.

2.1.3 Jets

As mentioned, quarks have color charge. There exist three different color charges: red (R); green (G); blue (B). Quarks can not exist as color-charged states as free particles. Instead, they are confined into hadrons. These are called colorless, which means that the color of each quark in the hadron cancel. This can be done by either having one of each color, which creates "white" color, or by having a color-anticolor pair. A hadron consists of valence quarks, which determine the characteristics of the hadron, sea quarks, which

are quark-antiquark pairs with canceling color charge, and gluons. Hadrons are divided into baryons, containing three valence quarks, and mesons, consisting of two [5].

At the LHC protons collide at a center of mass energy equal to 13 TeV [9]. This is enough energy to probe the proton and having a quark from each proton to interact instead of the protons as a whole. The collision can yield enough energy for the quarks in the collision to leave the hadrons. However, the physics behind the strong interaction called quantum chromo dynamics (QCD) causes the attractive force between quarks to increase with distance [5]. This effect is called asymptotic freedom and is caused by the fact that gluons also carry color charge. A gluon carries more than one color charge and switches the color between the interacting quarks. Since gluons couple to color charge it means that they can couple to each other (this is different from the EM interaction where the photon is chargeless and can not couple to itself). When the distance between two quarks increase there can be additional interactions between the gluons that carry the force between the two quarks. It is also possible to have gluon loops, shown in figure 3, in the interaction. Since gluons couple, a gluon can decay into a pair of gluons that recombine back into a gluon. This is what is called a loop. There also exist loops in the form of quark-antiquark pairs and for QED there exist electron-positron pairs. A quark or electron loop will weaken the interaction. This is called screening and can be seen as the charge of the particles shielding the charge between the two interacting particles. However, gluon loops will increase the charge between two interacting quarks and thus also increase the strength of the interaction. This effect is called antiscreening [8].

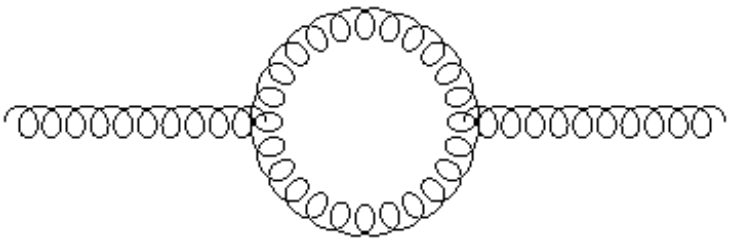

Figure 3: Feynman diagram of a gluon loop.

Eventually there will be enough energy to create a quark and anti-quark pair. In a simplified picture this can be seen as the escaping quark becoming bound in a colorless state with one of the new quarks. The other new quark becomes bound in the original hadron. Because of this, the escaping quark is no longer bound to the original hadron, but is instead confined within a new hadron. This can happen more than once after a collision and this chaotic phenomena is called hadronization. In hadronization new hadrons are created and this shower of hadrons is called a jet. In absence of other quarks and gluons nearby, each jet corresponds to one quark or one gluon and it is these that will be detected in the detector. The total energy of the jet corresponds to the energy of the initial quark or gluon [5].

2.2 Dark Matter

The SM is, however, not a complete model and there are experimental observations that are not explained by the model. One such observation is dark matter, which is non-luminous matter. Astronomical observations provide compelling proof that dark matter is a substantial part of our universe. These observations also suggest that dark matter is non-baryonic and are thus not included in the SM [1].

2.2.1 Cosmological Evidence

In the 1930's, Jan Oort used Doppler shifts to measure that stars in the Milky Way move fast enough to escape the luminous gravitational pull of the galaxy. This suggest that there might exist matter within the Milky Way that is non-luminous and adds enough gravitational pull to keep the stars in orbit. Around the same time, astronomer Fritz Zwicky studied the Coma cluster (322 million light-years from Earth) by measuring the Doppler shifts of the galaxies in the cluster. This way he could calculate the velocity dispersion of the galaxies, which corresponds to their kinetic energy. From his result Zwicky calculated the average mass of a nebula in the Coma cluster $M_{nebula} = 4.5 \cdot 10^{10} M_{\odot}$ ($M_{\odot}$ denotes mass of the Sun). A cluster, containing approximately thousand nebulae, has the total mass $M_{nebula} \approx 4.5 \cdot 10^{13} M_{\odot}$. The mass of the cluster can also be measured with mass M over luminosity L ratios. For a certain body there exists a well-defined M/L ratio which makes it possible to find the mass if its luminosity is known. The mass of the Coma cluster calculated with this method was 10% of the value Zwicky found using the velocity dispersion. Hence, both Oort and Zwicky found a large amount of mass that could not be seen.

The presence of this non-luminous mass was confirmed by Vera Rubin. She measured the rotation curves of 60 distant galaxies. If one assumes that the galaxies orbits behave like planets around a star their rotational velocities $v(r)$ can be expressed using:

$$v(r) = \sqrt{G * \frac{m(r)}{r}} \tag{2}$$

where G is the gravitational constant and $m(r)$ is the total mass within radius r. Equation 2 will decrease with increasing r if no new mass is introduced. Since the luminous mass is concentrated in the center of spiral galaxies it is expected that $v(r)$ will eventually decrease with distance. This is not seen, however, instead the value flattens out. This suggests that more mass is present at increasing r. Hence, non-luminous mass is not concentrated at the center [1].

2.2.2 Non-Baryonic Dark Matter

Through measurements of the Cosmic Microwave Background (CMB) it is possible to show that the missing mass should not consist entirely of baryonic matter. The CMB is

an excess of background temperature equal to 2.73 K. After the Big Bang the universe was a dense plasma of charged particles and photons. After this plasma had cooled, neutral atoms started to form. This is called the epoch of recombination. The universe became transparent to electromagnetic radiation and photons started to flow freely in the universe. These photons exist today as the CMB.

The CMB is extremely uniform, but there exist some small fluctuations. The fluctuations depend on the amount of baryons in the universe at the time of recombination. Before recombination, the photons and protons in the plasma can be modeled as a fluid called photon-baryon fluid. This fluid compresses as it goes deeper into a gravitational well. The pressure of the fluid will increase and the fluid starts expanding. This expansion causes the pressure to decrease, so it starts to compress again. Depending on where the photons decouple in this loop, the energy of the photons will change. Inside the gravitational well the photons need to escape a larger potential and will thus have less energy. The Cosmic Background Explorer [10] measured these fluctuations and they were found to be surprisingly small, about 30 μK. This was not enough for the universe to have formed as we see today in a purely baryonic universe. Baryonic matter only become charge neutral at the epoch of recombination. This means that it can not form gravitational wells before the recombination because of electrostatic forces preventing the matter to clump together. Thus an electromagnetically neutral matter is needed to form gravitational wells before the epoch of recombination so that structure formation could begin early in the universe.

More precise measurements were performed in 2001 by the Wilkinson Microwave Anisotropy Probe [11]. From this the total matter density $\Omega_m h^2$ was found to be equal to $0.1335^{+0.0056}_{-0.0055}$ and baryon matter density $\Omega_b h^2$ equal to 0.02260 ± 0.00053. Here Ω_i is the density of i relative to a critical density and h is the Hubble constant. This means that baryonic matter makes up approximately 6% of the total matter in the universe. From N-body simulations, simulation of n particles with pair-wise interaction [12], of the matter distribution in the universe on a large scale (Large Scale Structure) [13] it is possible to see that a universe with relativistic dark matter slows down the structure formation. Because of this dark matter needs to be non-relativistic or "cold" during structure formation [1].

2.3 Weakly Interacting Massive Particles

The only evidence of dark matter interacting with SM so far is through gravity, but there is a possibility that these particles can interact weakly using some other force as well [14]. If it is assumed that the DM is around the weak scale (246 GeV [1]) and if the coupling strength is comparable to the coupling of electroweak interactions, then an approximate value for the DM relic abundance can be predicted which closely matches the observed astronomical value. If DM is weakly interacting with SM then they are in thermal equilibrium during the early universe. This gives an easy initial condition for the evolution of DM abundances. Such DM candidates are called weakly interacting massive

particles (WIMP) and the matching relic abundances is simply called the WIMP miracle [15]. There are numerous theories for WIMP candidates, but in order for the results to be as general as possible no specific model has been used.

2.4 Detection at Colliders

This thesis focuses on searches at the ATLAS detector (seen in figure 4). It is a cylindrical detector built in layers as most other particle detectors. The first layer is a tracking detector that tracks charged particles. A magnetic field is applied so that the charge of the particle can be determined. Next layer is an electromagnetic calorimeter that measures the energy of charged particles. After that are the hadron calorimeters which detects energies of particles using strong interaction. The last layer consist of muon chambers. Only muons are energetic enough to reach these detectors and a detection here is thus certain to be a muon [8].

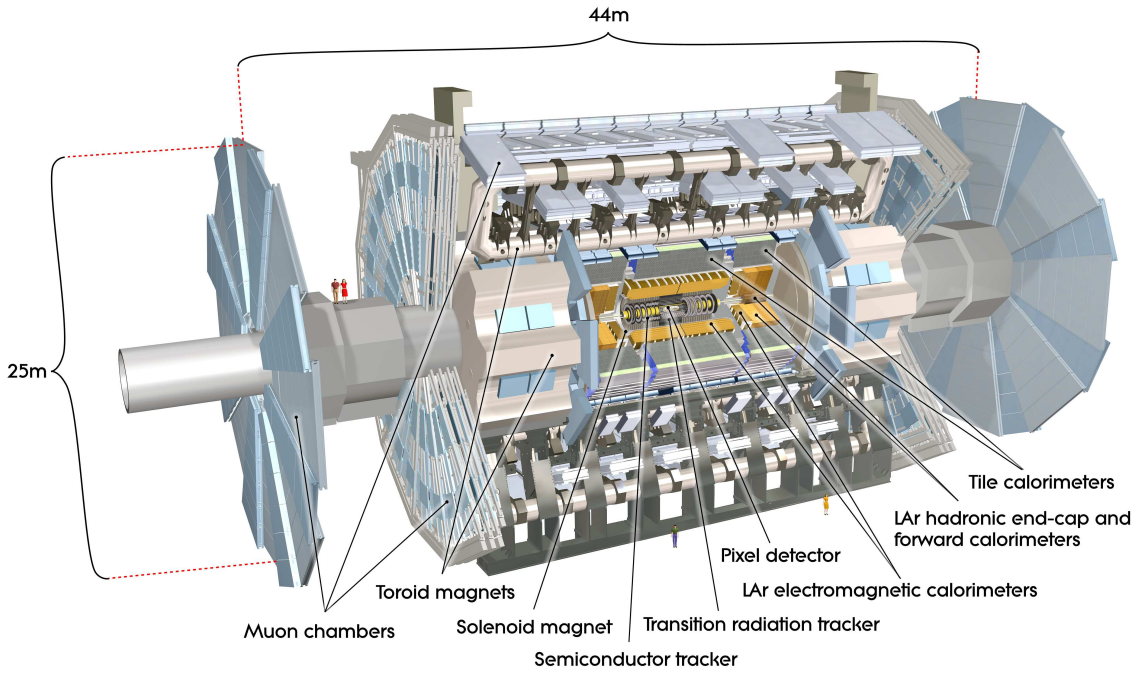

Figure 4: Cut-away view of the ATLAS detector [16].

Since WIMPs are weakly interacting they will pass detectors undetected, similarly to neutrinos, unless the detectors are especially designed to detect weakly interacting particles. There exist experiments that try to detect WIMPs directly [1] exploiting the recoil of the nucleus after an interaction with a WIMP, but at the LHC these particles will be detected indirectly. Figure 5a depicts a basic SM to DM interaction. A DM interaction

event in the simplest models of dark matter [17] can appear in two ways, depending on the decay of the particle that mediates the DM interaction. A *mono-X event* (seen in figure 5b) will be seen as a SM particle or jet from initial state radiation recoiling against the invisible DM particle, leading to missing transverse momentum, which is the missing momentum perpendicular to the beam direction [18]. A *di-X event* (seen in figure 5c) will occur if two SM particles annihilate to the dark matter mediator and the mediator decays back into two SM particles. In this thesis, I study the case in which the mediator decays into a pair of quarks (*di-jet*).

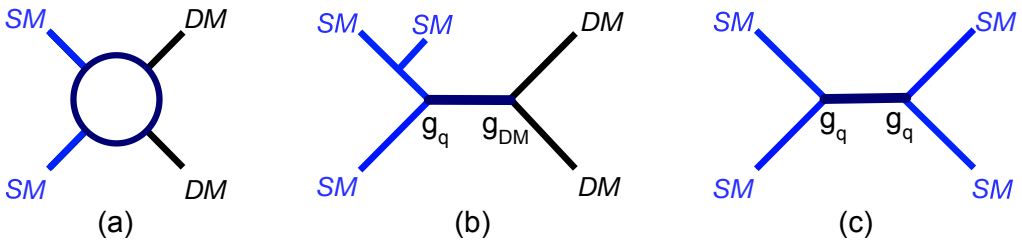

Figure 5: Feynman diagrams of possible DM events in a collider. (a) is a basic SM to DM interaction, (b) is a *mono-X event* and will be seen as missing transverse momentum and (c) is a *di-X event* and will give an increase in event counts around the DM mediator mass. [19]

In a *di-X event* no missing momentum will be seen and the invariant mass m_{jj} of the two jets or leptons can be calculated. When plotting the number of events as a function of the invariant mass there will be a peak at the mediator mass [6]. From energy conservation m_{jj} can be expressed as:

$$m_{jj}^2 = (E_1 + E_2)^2 - (\mathbf{p}_1 + \mathbf{p}_2)^2 = E_{MED}^2 - \mathbf{p}_{MED}^2 = m_{MED}^2 \tag{3}$$

where E_1, E_2, $\mathbf{p}_1$ and $\mathbf{p}_2$ are the energies and momentum of the two SM particle decay products of the DM mediator. E_{MED} is the energy, $\mathbf{p}_{MED}$ is the momentum and m_{MED} is the mass of the mediator. From equation 3, $m_{jj} = m_{MED}$. Because of this, there is an increase of events in the form of a peak around the mediator mass and this is called a resonance. The shape of the peak is approximately given by the Breit-Wigner formula:

$$N(m_{jj}) = \frac{K}{(m_{jj} - m_{MED})^2 + (\Gamma^2/4)}$$

where $N(m_{jj})$ is the number events at a certain invariant mass and K is a constant depending on the total number of events detected. Γ is the decay width that is defined as

the invariant of the mean lifetime τ and will be equal to the full width at half maximum (FWHM) of the peak. The center of the peak will be at m_{MED}. If no bump is seen, we can interpret the lack of events as a constraint on the parameters of dark matter models [6].

2.5 Monte Carlo Generation

In an interaction between two hadrons there are many factors affecting the result. Firstly, it is possible for more than one parton-parton interaction to occur in one collision. Secondly, there will be initial- and final-state radiation. Lastly, the partons involved will take part in hadronization and create more hadrons bunched together in a jet. Each particle hitting the detector have approximately 10 degrees of freedom: mass; flavor; momentum; production vertex; lifetime; etc. Also, some phenomena like hadronization are not fully understood and no analytical expression exists. Thus it is necessary to generate the events in a MC generator.

It is possible to calculate the matrix elements M_{fi} of the interaction. This in turn, together with the phase space, is used to calculate the cross-section as in equation 1. Our model is generated by MadGraph5 at leading order (LO), where these calculations are trivial. For simulations done at next-to-leading order (NLO) and beyond the calculations become increasingly difficult. This is caused by further decay possibilities (e.g. three decay products) and loops. These both lead to divergences and only cancel if both are taken into account.

It is possible to have, for example, emitted gluons after or before the interaction and this is called final- and initial-state radiation (FSR and ISR respectively). These can be explained with the shower approach. For FSR the interaction is seen as one separate event, after this the decay products are followed and if one of these emit another parton this is seen as a new interaction in which the decay product is replaced by two partons. For ISR one need to use the parton distribution function in order to calculate. It is interpreted as the hadron splitting up more the closer it gets to the interaction. If there is an interaction there will be ISR, otherwise the hadron recombines. Because of this the MC generator generate backwards in time from the interaction. The program calculates what could have happened before the given interaction. There will be more than one possibility, but one is randomly chosen.

Using matrix elements is good for well separated jets and allows for expansion in powers of α_s leading to higher precision. On the other hand, it is not good at loops and internal structure of jets. These things are instead better explained with parton showers. Thus it is desired to combine these two methods to complement each other. This is done in PYTHIA [20], which provides parton showers for the matrix elements generated by MadGraph5.

The generation gets further complicated by the fact that there can be more than one parton interaction in a collision and that the decay products will undergo hadronization.

Multiple parton interactions are handled by for example assuming that they are created in ordered sequence with decreasing transverse momentum. Hadronization is not fully understood and has to be generated using simple models that are fixed afterwards using observations from experiments to get physical results [21].

2.6 Summary Plot

Current searches for DM place constraints on existing models. By comparing simulations and theoretical models with experimental data it is possible to limit the region of parameter space of DM models in which dark matter can still be found. Figure 6 shows a summary plot that is a combination of all constraints from ATLAS *mono-X* and *di-jet* searches. The plot has dark matter mass m_{DM} on the y-axis and m_{MED} on the x-axis. The couplings to DM g_{DM} and quarks g_q are axial-vector couplings [5] and fixed to $g_{DM} = 1$ and $g_q = 0.25$ and the coupling to leptons is zero.

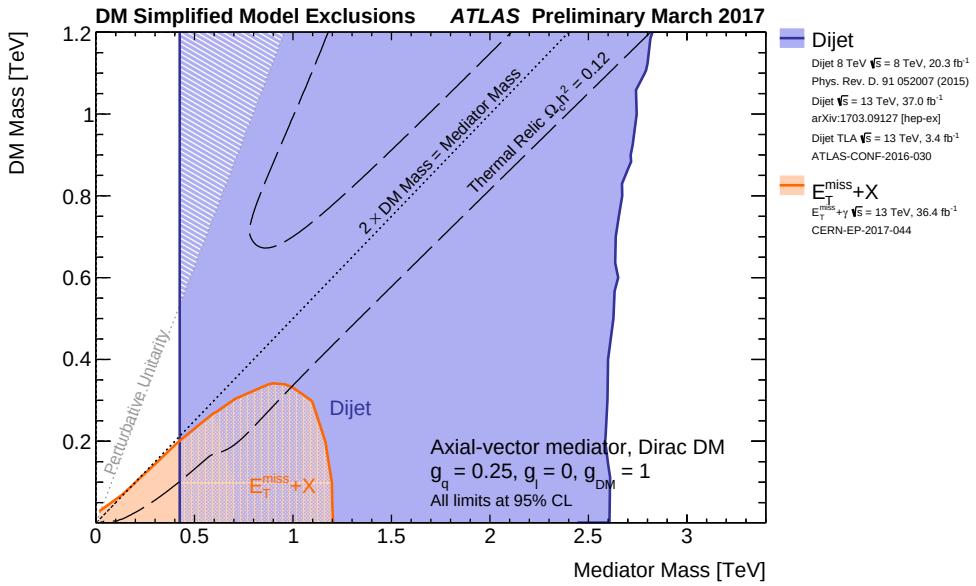

Figure 6: Summary plot on DM constraints. Highlighted areas have been excluded [22].

Theoretical models are tested either analytically or through simulations. A theory model provides an estimate for a cross section σ_{theo} for a given DM signal [5]. σ_{theo} is compared to the number of events produced by a possible signal that are excluded by experimental results. This number of events is proportional to the excluded cross section σ_{exp}. There are kinematical selections, which enhance the signal with respect to the background, applied to the number of events σ_{exp}. Because of this, σ_{theo} needs to be multiplied by the acceptance, which is defined as the ratio of events after and before applied selections. If

σ_{exp} is smaller than σ_{theo}, the theoretical model would predict more events than there are observed, and it can be excluded [23].

The summary plot has four different components. The areas named Dijet and $E_T^{miss} + X$ have been excluded using *di-jet* and *mono-X event* searches. The surface enclosed within the dashed lines are based on the relic density, which is the density of a specific particle after thermal equilibrium was broken during the early universe [1]. The relic density was calculated for the parameters of the model and the lines enclose the surface with the correct values assuming that the model considered constitutes all of the DM in the universe [24]. The perturbative unitarity line is given by [23]:

$$m_{DM} = \sqrt{\frac{\pi}{2}} m_{MED} g_{DM}^{-1}$$

Everything behind this line is not theoretically allowed. The mass surfaces that are excluded depend on the parameters of the model. Thus, figure 6 applies only for the case with $g_{DM} = 1$ and $g_q = 0.25$.

3 Method

The summary plot described in the previous section needs the generation of events for each point in DM and mediator mass to obtain the theoretical cross section and to compare the theory with the data. In this work, the same procedure and software used in the ATLAS experiment has been followed in order to generate a number of signal points.

Dark matter *di-jet events* were generated at both TRUTH and simulated at the detector level. TRUTH level consists of both the matrix element describing the parton-parton interaction done in MadGraph5 and parton showers (particle level) done in PYTHIA as in figure 7. At the detector level, simulation of the interactions of particle with the detector matter is done using Geant4 [25], a software program that simulates particle interactions in matter.

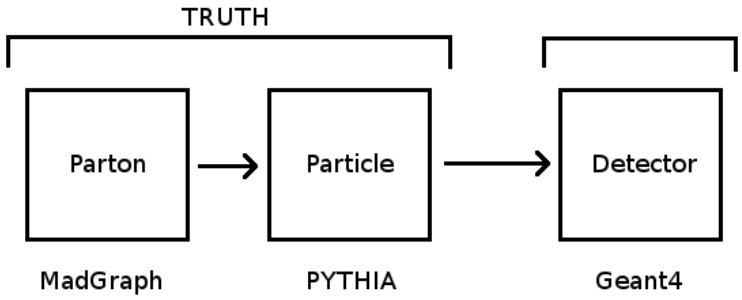

Figure 7: The different steps of generating events.

A resonance at parton level will have a mass given by the energies of the partons. At particle level there will be a smearing to the true particle energy caused by the parton showers. For detector level, the measurement of particles in a detector introduces further smearing. The extent of this smearing is called resolution. A detected peak with a Gaussian distribution (see equation 7 in section 3.2) will have energy resolution ΔE equal to the FWHM, which is given by equation:

$$\text{FWHM} = 2.35\sigma$$

where σ is the standard deviation of the Gaussian peak. Energies closer than ΔE can not be resolved [26]. The detector resolution is not included at TRUTH level. Instead, the simulated jets are smeared using the values in figure 8 to approximate the uncertainty in the detector. Figure 8 shows the resolution of the ATLAS detector for a *di-jet event*. Here the y-axis is the relative mass resolution σ_{rel} given by:

$$\sigma_{rel} = \frac{\sigma_{m_{jj}}}{m_{jj}}$$

where $\sigma_{m_{jj}}$ is the mass resolution of a certain invariant mass m_{jj}. On the x-axis is the invariant mass.

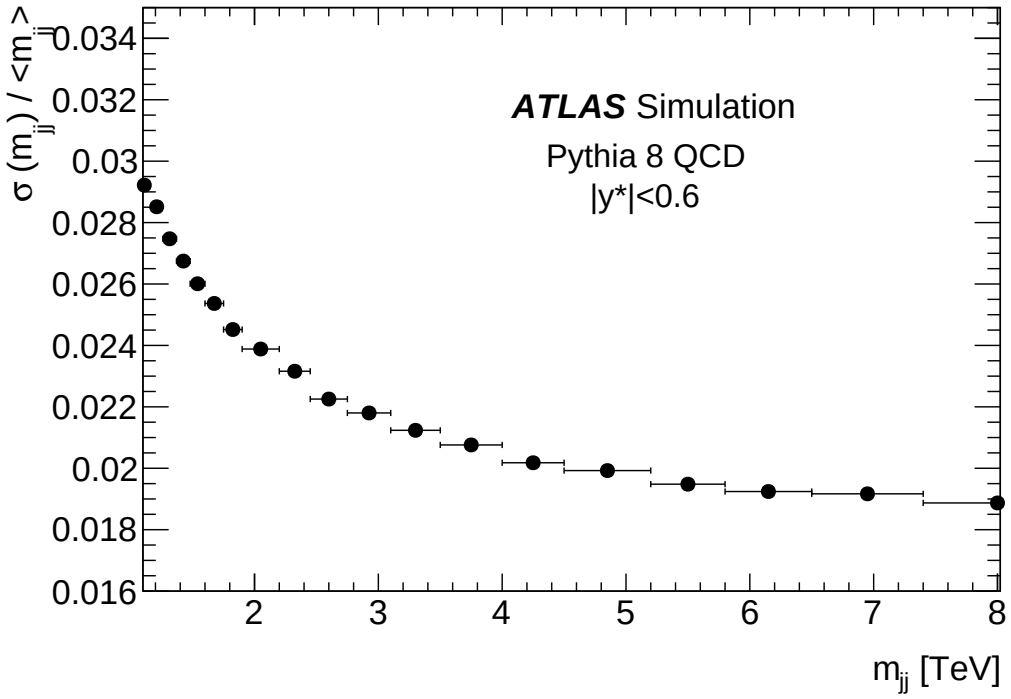

Figure 8: Relative mass resolution as a function of invariant mass [27].

The smeared TRUTH level was compared to the more involved detector level generation to determine if the smearing is a good approximation.

Since the search for dijet resonances relies on identifying a peak above a continuous background [6], it is important to estimate the effects of the experimental resolution when interpreting the results towards a summary plot. If the effects of the resolution can be parameterized, then one does not need to execute the full simulation of the interactions of particles with matter.

3.1 Dark Matter model generated

The model generated represents an axial-vector mediator that carries the force between DM and SM particles. All simulations used these values:

- $g_{DM}^{A} = 1.5$
- $g_{q}^{A} = 0.1$
- $m_{DM} = 10$ TeV
- $\sqrt{s} = 13$ TeV

for the coupling constant g_{DM}^{A} with DM, g_{q}^{A} with quarks, the mass of the dark matter particle and the center of mass energy. The mediator does not couple to leptons. Three different values for m_{MED} equal to 650 GeV, 1 TeV and 2 TeV were generated. These masses where chosen since different detector effects are present at low, intermediate and high masses as seen in figure 8. All mediator masses are less than $2m_{DM}$ and are thus off-shell with respect to dark matter. For DM interactions, the mediator will be a virtual particle, and hence off-shell, since it violates energy conservation. In order to bypass the violation the particle only exists for a short enough time to be undetected [8]. The mediator will be on-shell (or real) with respect to quarks. Because of this, the mediator created in the collision will only be able to decay into quarks.

3.2 TRUTH Level VS Detector Level

20,000 events were generated at both TRUTH and detector level for the three different mediator masses in section 3.1. In order to reduce background in the search for dark matter mediator particles in the *di-jet* final state, different selection were applied to the generated events. The first selection was applied on the rapidity difference y^*:

$$y^* = \frac{y_1 - y_2}{2} \tag{4}$$

where y_1 is the rapidity of the leading jet and y_2 of the subleading jet. Rapidity y is defined as:

$$y = -\ln\left(\tan\left(\frac{E+p_z}{E-p_z}\right)\right) \tag{5}$$

where E is the energy of the particle and p_z is the z-component of the momentum. There is a momentum imbalance because of the different fraction of total momentum carried by the two partons in the interaction. However, y^* is invariant of this momentum imbalance [28]. y^* was calculated using another useful quantity which is pseudorapidity η. It is defined as:

$$\eta = -\ln\left(\tan\left(\frac{\theta}{2}\right)\right)$$

where θ is the angle between the direction of the momentum $\boldsymbol{p}$ of the particle and the beam axis. Pseudorapidity can also be expressed:

$$\eta = -\ln\left(\tan\left(\frac{|\boldsymbol{p}|+p_z}{|\boldsymbol{p}|-p_z}\right)\right) \tag{6}$$

For large momentum the mass is negligible, and then $|\boldsymbol{p}| \approx E$. Then equation 6 can be approximated as equation 5 and a cut in pseudorapidity is the same as a cut in rapidity [29]. The pseudorapidity of each jet was given by MadGraph5 and equation 4 was thus calculated by using the pseudorapidity of the jets instead of their rapidity. Most new physics scenarios produce central jets in the laboratory frame, which means that the rapidity difference is small, and thus only events with $y^* < 0.6$ were selected. The second selection was on the minimum transverse momentum, which was $p_t > 220$ GeV. This was done since events from QCD under a certain threshold can not be recorded in the ATLAS detector because of data storage restrictions [30].

The invariant mass m_{jj} was calculated for each event with:

$$m_{jj} = |jet_1 + jet_2|$$

where jet_1 is the Lorentz vector of the leading jet and jet_2 is the Lorentz vector for the subleading jet. Each invariant mass is added as a count in a histogram.

Three m_{jj} histograms were created for each mediator mass: TRUTH level without smearing; TRUTH level with smearing; detector level. The histograms were scaled such that 1 on the y-axis counts as the total number of events generated before selections were applied. Thus the y-axis represent the percentage of events whose leading and subleading jets had a certain invariant mass. The histograms were fitted with three different functions. The first function f_G was a Gaussian with the form:

$$f_G = Ae^{-0.5\left(\frac{x-x_{peak}}{\sigma}\right)^2} \tag{7}$$

where A is the peak amplitude, x_{peak} is the peak position and σ is the standard deviation. The second function f_C is a Crystal Ball function [31] with the expression:

$$f_C = \begin{cases} A\left(\frac{n}{|\alpha|}\right)^n \frac{e^{-\frac{\alpha^2}{2}}}{\left(\frac{n}{|\alpha|}-|\alpha|-\frac{x-x_{peak}}{\sigma}\right)^n}, & \text{if } \frac{x-x_{peak}}{\sigma} < -\alpha \\ Ae^{-0.5\left(\frac{x-x_{peak}}{\sigma}\right)^2}, & \text{otherwise} \end{cases} \tag{8}$$

here A, x_{peak} and σ are akin to the variables with the same name for the Gaussian function. The last function f_{GL} is a superposition of a Gaussian and a reverse Landau function:

$$f_{GL} = A(f \cdot Gaussian(x, x_{peak}, \sigma_G) + (1-f) \cdot Landau(-x, x_{mpv}, \sigma_L)) \tag{9}$$

where A is the amplitude and f is a fraction. $Gaussian(x, x_{peak}, \sigma_G)$ is a Gaussian function dependent on x, the peak position x_{peak} and the width σ_G. $Landau(-x, x_{mpv}, \sigma_L)$ is a reverse Landau function dependent on x, the most probable value of x x_{mpv} and a different width σ_L. The total width σ_{GL} for f_{GL} was calculated with:

$$\sigma_{GL} = f \cdot \sigma_G + (1-f)\sigma_L \tag{10}$$

Relative widths σ_{rel}, which are the widths from the fitted functions divided by m_{MED}, were calculated. The relative widths were analyzed by adding them to plots (seen in figure 12) with m_{MED} as the x-axis for each fit function. To check the quality of the fitted functions the relative chi-square value χ^2_{rel} [32] were also calculated. The dependence between the quality of the fits and the bin size was not investigated.

4 Results

The histograms with mediator mass equal to 2 TeV are seen in figure 9, equal to 1 TeV in figure 10 and equal to 650 GeV in figure 11. The figures depict percentage of detected events as a function of intermediate mass (see section 3.2). For all histograms the peak position is around m_{MED} as expected. Figures 9-11 consist of three figures, where the histograms are fitted with a Gaussian function in figure a, with a Crystal Ball function in figure b and with a Gaussian + reverse Landau function in figure c (equations 7-9).

The Gaussian function and Gaussian + reverse Landau function fits in figures 9a and 9c respectively both matches the three different histograms fairly well. The Crystal Ball function fit is also an okay match for both detector level and TRUTH level with smearing, but does not have the same amplitude as the histogram without smearing, as seen in figure 9b.

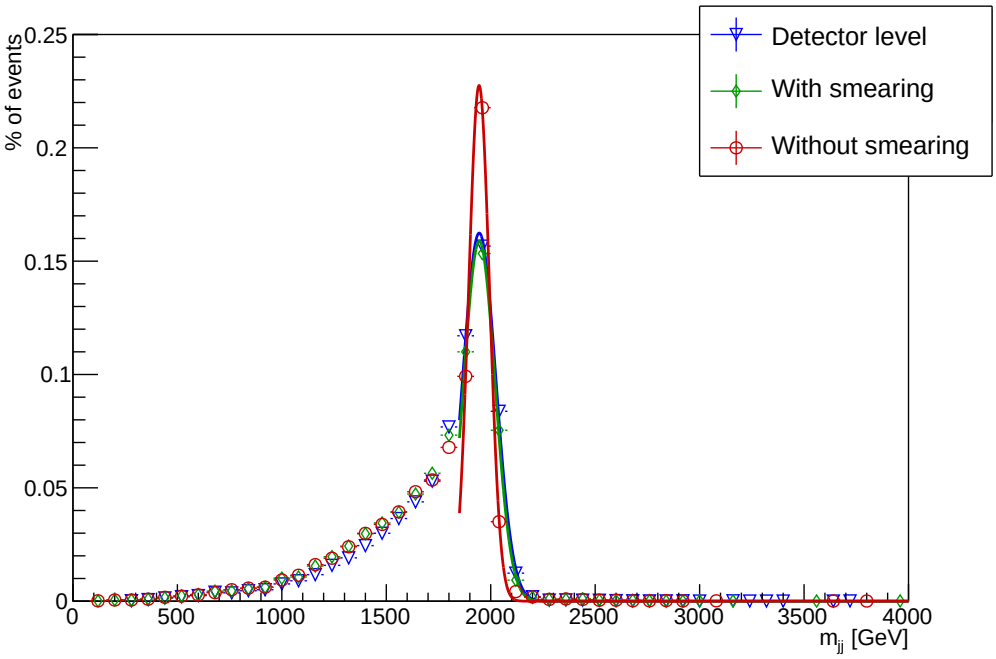

(a) Gaussian function

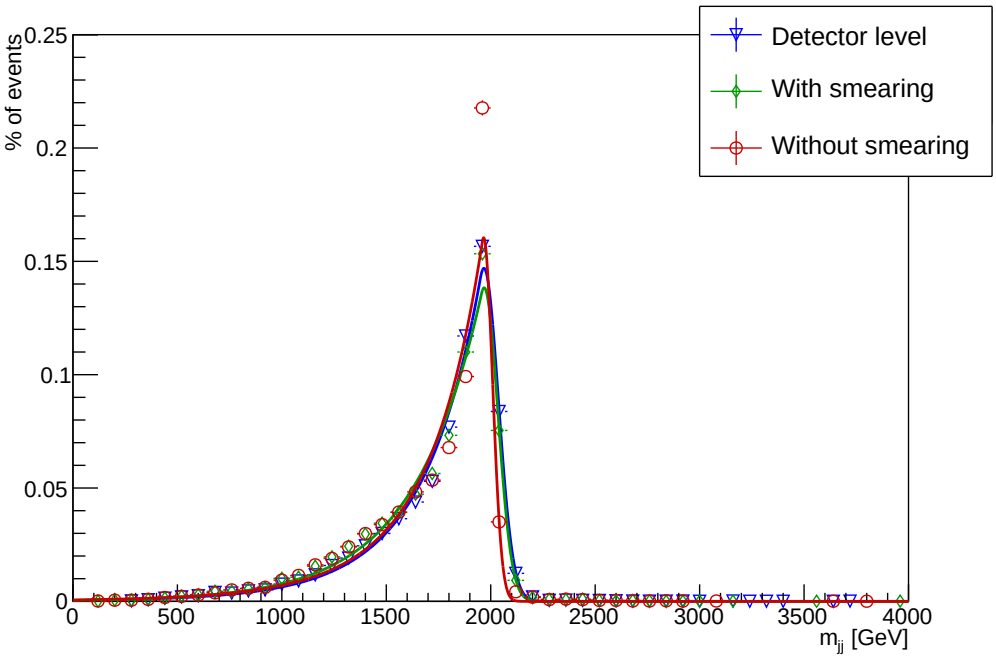

(b) Crystal Ball function

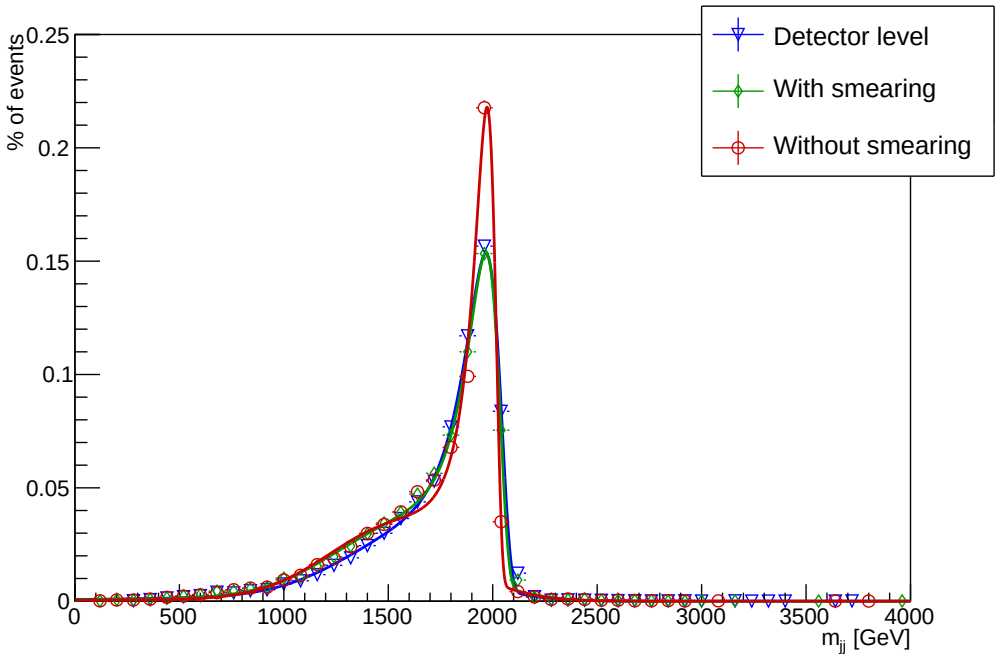

(c) Gaussian + reverse Landau function

Figure 9: Histograms with percentage of events on the y-axis and invariant mass on the x-axis for 2 TeV mediator mass fitted with three different functions.

For histograms with $m_{MED} = 1$ TeV both the Gaussian function and Crystal Ball function matches the histograms as seen in figures 10a and 10b. However, the Gaussian + reverse Landau function is not a good fit for any of the histograms, which is seen in figure 10c.

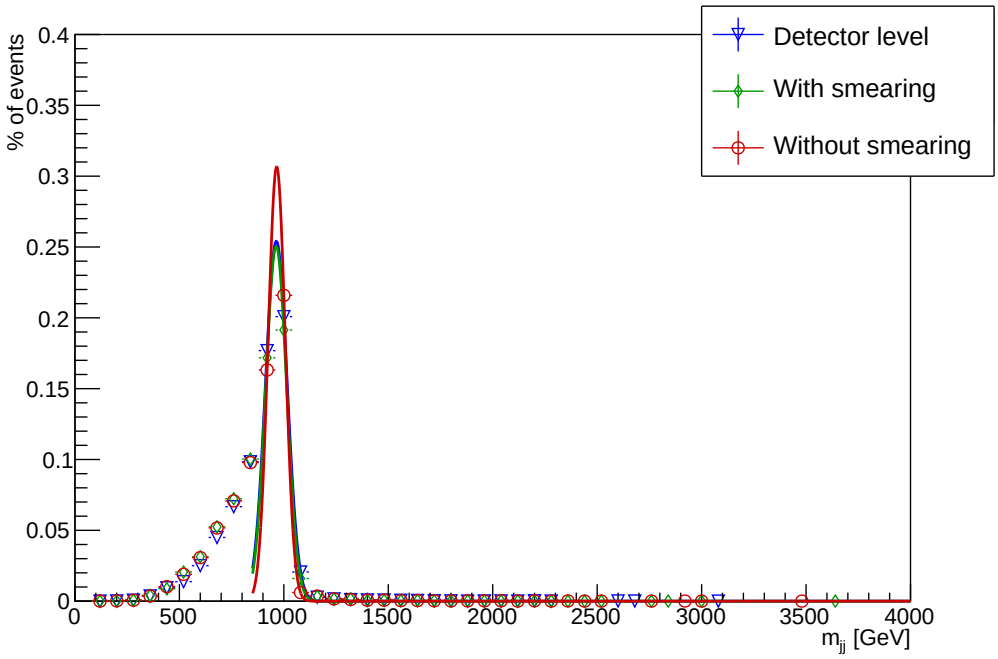

(a) Gaussian function

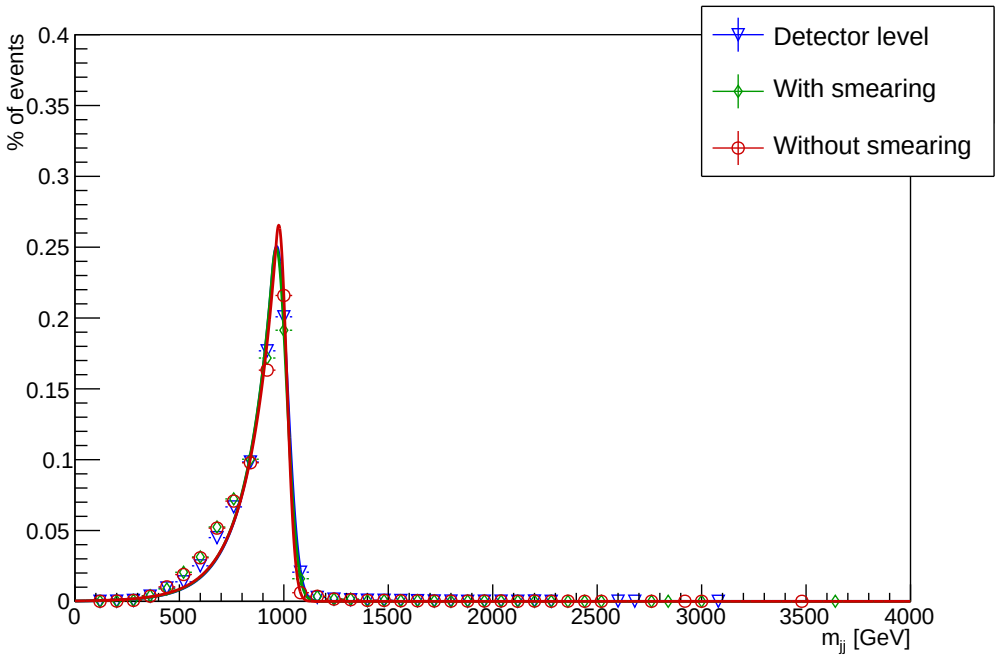

(b) Crystal Ball function

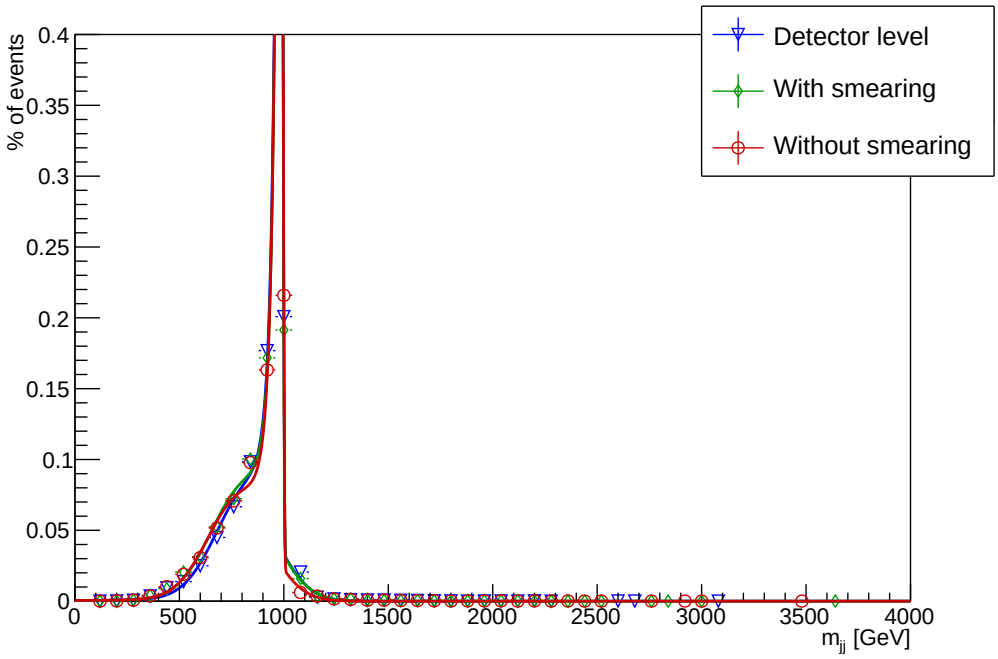

(c) Gaussian + reverse landau function

Figure 10: Histograms with percentage of events on the y-axis and invariant mass on the x-axis for 1 TeV mediator mass fitted with three different functions.

The histograms with mediator mass equal to 650 GeV are fitted well with the Gaussian (figure 11a) and Crystal Ball (figure 11b) functions, but not by the Gaussian + reverse Landau function (figure 11c) as for 1 TeV m_{MED}.

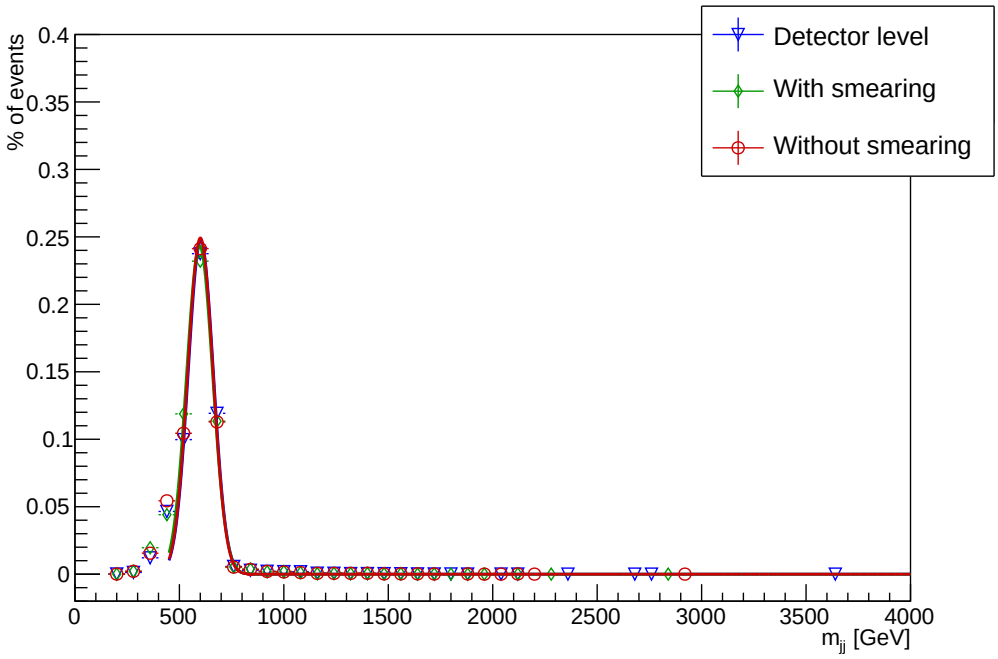

(a) Gaussian function

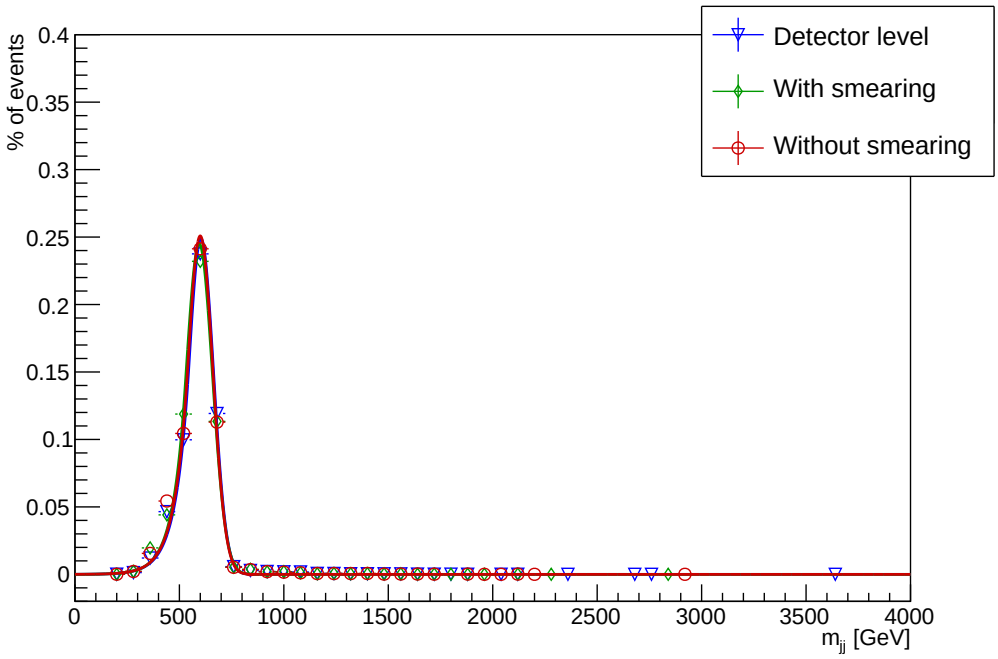

(b) Crystal Ball function

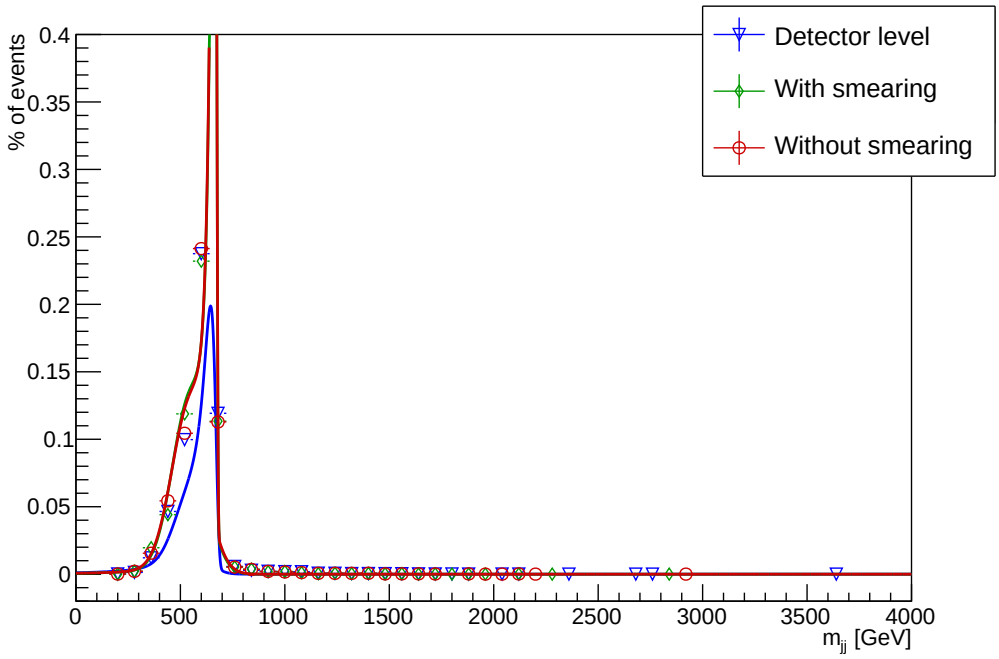

(c) Gaussian + reverse landau function

Figure 11: Histograms with percentage of events on the y-axis and invariant mass on the x-axis for 650 GeV mediator mass fitted with three different functions.

As can be seen all histograms are reasonably well fitted with a Gaussian function. The Crystal Ball function fits all histograms except for the histogram with 2 TeV mediator and no smearing. The Gaussian + reverse Landau function is a good fit for the histograms at 2 TeV mediator mass, but it does not provide a good fit for the histograms with the other mediator masses. This can be further illustrated by the χ^2_{red} values in table 1.

Table 1: χ^2_{red} for all fits.

mMED	**Histogram**	**Gaussian** χ^2_{red}	**Crystal Ball** χ^2_{red}	**Gaus.+R.Land.** χ^2_{red}
2000 GeV	TRUTH without Smearing	13.2	29.0	8.2
	TRUTH with Smearing	7.5	10.6	7.2
	Detector Level	4.6	7.2	7.9
1000 GeV	TRUTH without Smearing	9.2	31.2	13.2
	TRUTH with Smearing	9.2	33.7	12.7
	Detector Level	10.0	23.8	16.3
650 GeV	TRUTH without Smearing	14.5	30.1	56.3
	TRUTH with Smearing	16.5	27.3	55.7
	Detector Level	13.8	21.5	149.1

From this table it is possible to see that the χ^2_{red} values are generally better for higher

m_{MED}. This could be caused by the fact that the peak shape is more prominent at higher energies making the fit easier. The average value for the Gaussian fits is 11.0, for the Crystal Ball fits it is 23.8 and it is 36.3 for the Gaussian + reverse Landau fits. Thus it can be argued that histograms are fitted the best with the Gaussian function. The Gaussian + reverse Landau function χ^2_{red} values are fairly small for mediator mass equal to 1 TeV. This is surprising, since by looking at figure 10c it is clear that the fit is not a good representation of the histogram.

The relative widths are listed in table 2 where it is possible to compare widths for different mediator mass, which level the events were generated at and which function was used. The table includes the total relative width of the Gaussian + reverse Landau function fits, calculated by dividing equation 10 with the mediator mass. It also includes the width of the Gaussian function part σ_G and the reverse Landau function part σ_L of the Gaussian + reverse Landau function fit.

Table 2: The relative width values with error for all fitted histograms. Here σ_{GL} represent the total relative width of the Gaussian + reverse Landau function. σ_G is the relative width of the Gaussian function in the function and σ_L is the width of the reverse Landau.

mMED	Histogram	Gaussian σ_{rel}	Crystal Ball σ_{rel}	σ_{GL}	σ_G	σ_L
2000 GeV	TRUTH without Smearing	0.0250 ± 0.0003	0.0214 ± 0.0005	0.0683 ± 0.0004	0.1591 ± 0.0024	0.0167 ± 0.0003
	TRUTH with Smearing	0.0377 ± 0.0005	0.0327 ± 0.0008	0.0702 ± 0.0006	0.1642 ± 0.0026	0.0253 ± 0.0006
	Detector Level	0.0398 ± 0.0006	0.0346 ± 0.0008	0.0576 ± 0.0010	0.1580 ± 0.0031	0.0279 ± 0.0010
1000 GeV	TRUTH without Smearing	0.0408 ± 0.0005	0.0380 ± 0.0007	0.0592 ± 0.0009	0.1512 ± 0.0018	0.0088 ± 0.0009
	TRUTH with Smearing	0.0499 ± 0.0007	0.0498 ± 0.0008	0.0678 ± 0.0008	0.1576 ± 0.0016	0.0085 ± 0.0008
	Detector Level	0.0520 ± 0.0007	0.0515 ± 0.0009	0.0607 ± 0.0009	0.1520 ± 0.0019	0.0086 ± 0.0008
650 GeV	TRUTH without Smearing	0.0924 ± 0.0008	0.0927 ± 0.0010	0.0591 ± 0.0007	0.1310 ± 0.0014	0.0125 ± 0.0007
	TRUTH with Smearing	0.0963 ± 0.0008	0.0973 ± 0.0009	0.0584 ± 0.0007	0.1272 ± 0.0017	0.0125 ± 0.0007
	Detector Level	0.0927 ± 0.0008	0.0917 ± 0.0011	0.0488 ± 0.1149	0.1118 ± 0.2004	0.0294 ± 0.0423

To further demonstrate the poor quality of the Gaussian + reverse Landau fits it can be remarked upon that the σ_G and σ_L have a large difference. One would expect these values to be fairly similar. Furthermore, the 650 GeV detector level σ_{GL} has larger error than its own value.

As mentioned in section 3.2 the widths are plotted in figure 12. In figure 12a the relative widths for the Gaussian functions are shown. These have similar values and distribution to the widths from the Crystal Ball functions in figure 12b which is a good sign because both functions seem to represent the histograms well. It can be seen that the widths for the different generation levels are fairly close, especially at lower mediator mass. Figure 12c that include the widths for the Gaussian + reverse Landau function does not resemble the other width plots because of the poor quality of the fits.

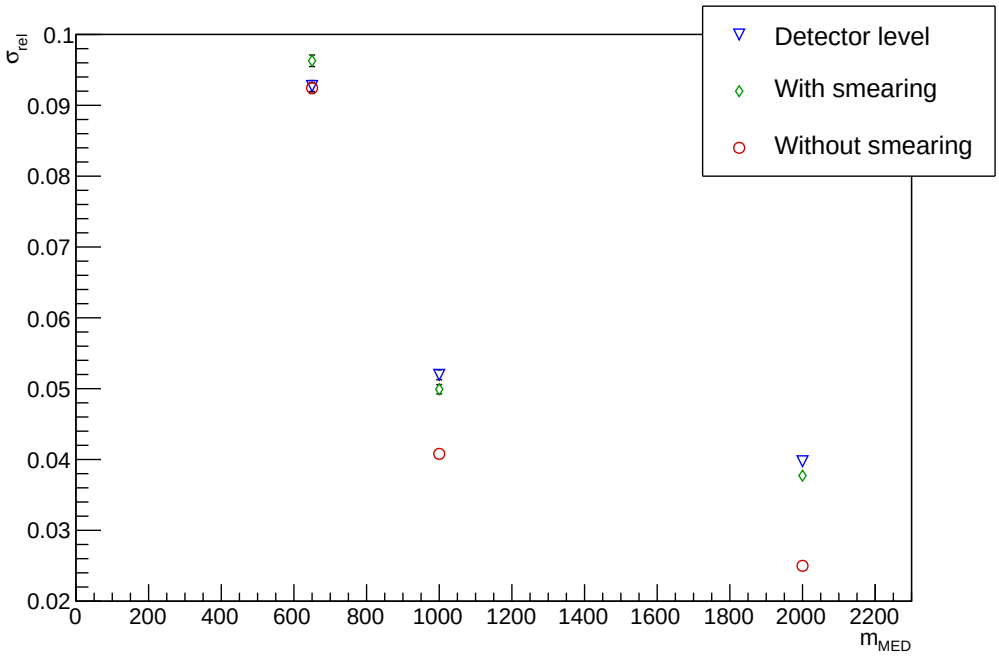

(a) Gaussian function

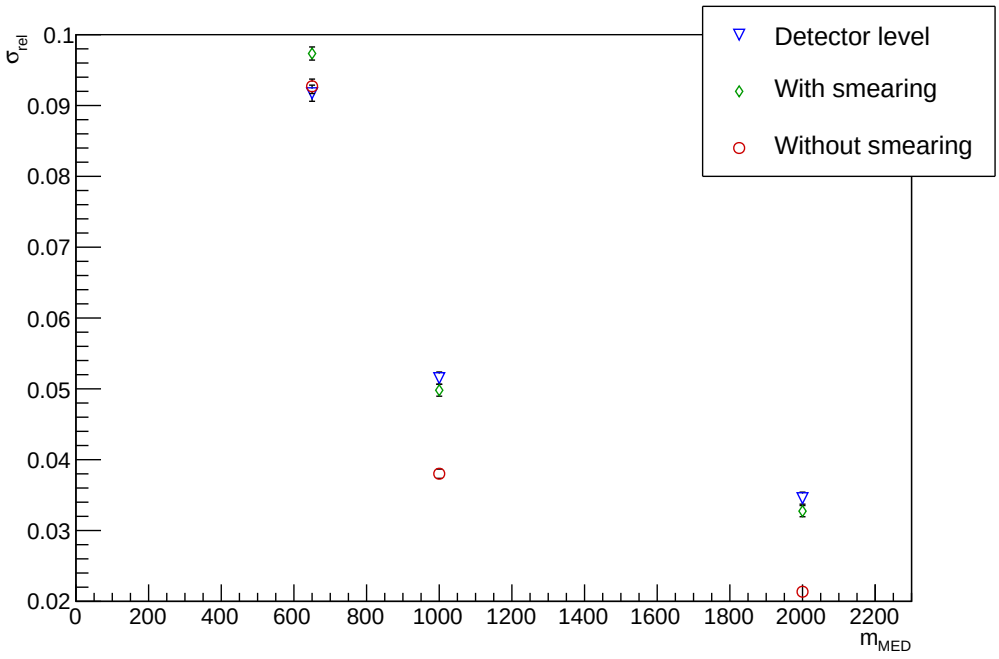

(b) Crystal Ball function

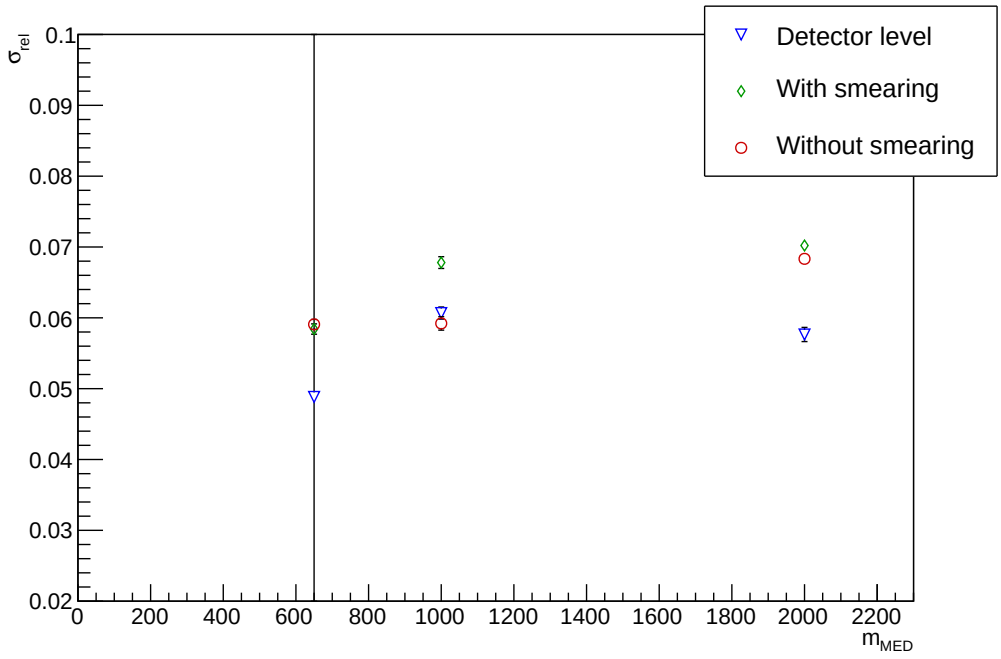

(c) Gaussian + reverse landau function

Figure 12: Relative widths (with error bars) of the fitted functions with mediator mass on the x-axis. Note the marker close to the x-axis in figure b.

Figure 12a and 12b seem to imply that the smearing might be a good approximation for the effects of the detector. Figure 12c can be discarded because of the bad quality of the fits. The error is larger for σ_{rel} from the Crystal Ball function than from the Gaussian function, which makes sense since the Crystal Ball χ^2_{red} value is also larger.

As mentioned in section 4, the relative width values are closer for low m_{jj}. Not only that, but the value is larger for smeared TRUTH level than for detector level. This means that the smearing is too big at low mass. At low mass the TRUTH level generations without smearing are a better match to detector level than the ones with smearing. The ratio $\Delta\sigma_{smear}$ between σ_{rel} for smeared events and detector level is given by:

$$\Delta\sigma_{smear} = \frac{(\sigma^G_{smear} + \sigma^C_{smear})}{(\sigma^G_{det} + \sigma^C_{det})} \tag{11}$$

where σ^G_{smear} is the relative width for the Gaussian fit to the smeared TRUTH level histogram, σ^C_{smear} is the same but for the Crystal Ball function fit and σ^G_{det} and σ^C_{det} is the same as σ^G_{smear} and σ^C_{smear} but for detector level histogram. The same expression but for TRUTH level without smearing will give $\Delta\sigma_{without}$:

$$\Delta\sigma_{without} = \frac{(\sigma^G_{without} + \sigma^C_{without})}{(\sigma^G_{det} + \sigma^C_{det})} \tag{12}$$

where $\sigma^G_{without}$ and $\sigma^C_{without}$ are the widths of the fits to the TRUTH level histogram without smearing. These two ratios are listed in table 3 for the different m_{MED}.

Table 3: $\Delta\sigma_{smear}$ is the average difference between the relative widths of detector level and of TRUTH level with smearing. $\Delta\sigma_{without}$ is the same but for TRUTH level without smearing.

mMED [GeV]	$\Delta\sigma_{smear}$	$\Delta\sigma_{without}$
2000	0.9480	0.6236
1000	0.9638	0.7617
650	1.0497	1.0037

5 Outlook

A large number of simulations are needed in order to test different theoretical models and produce summary plots. If the parameters of the model can be explained with an analytical formula or described with some approximation, then the generation time will decrease. This will benefit dark matter searches since an increased number of models can be examined in the same period of time.

From table 3 it is seen that $\Delta\sigma_{smear}$ is still close for $m_{MED} = 650$ GeV and can probably still be used even if TRUTH level without smearing is closer. For larger m_{MED} the smearing is closer to the detector level and is most likely a good approximation for the detector resolution. At these energies the smearing might be necessary for acceptable results.

This result may be used in future simulations of ATLAS *di-jet events* in order to decrease generation time. This will hopefully lead to an increased amount of data and larger constraints on dark matter models.

References

[1] K. Garrett and G. Duda, "Dark Matter: A Primer," *Adv. Astron.*, Jun. 2011.

[2] "Atlas." Internet: `https://home.cern/about/experiments/atlas`, 2012. [2017-05-02].

[3] "The large hadron colider." Internet: `http://home.cern/topics/large-hadron-collider`. [2017-03-12].

[4] J. Alwall *et al.*, "The automated computation of tree-level and next-to-leading order differential cross sections, and their matching to parton shower simulations," *Journal of High Energy Physics*, vol. 2014, no. 7, 2014.

[5] M. Thomson, *Modern Particle Physics*. Cambridge CB2 8BS, United Kingdom: Cambridge University Press, 6th ed., 2016.

[6] "A search for new physics processes using dijet events." Internet: `http://atlas.cern/updates/atlas-news/search-new-physics-processes-using-dijet-events`. [2017-03-12].

[7] MissMJ, "Standard model of elementary particles.svg." Internet: `https://commons.wikimedia.org/wiki/File:Standard_Model_of_Elementary_Particles.svg`, June 2006. [2017-04-13].

[8] B. Martin and G.Shaw, *Particle Physics: Third Edition*. The Atrium, Southern Gate, Chichester, West Sussex, PO19 8SQ, United Kingdom: John Wiley & Sons Ltd, 3 ed., Apr. 2009.

[9] K. Anthony, "Atlas completes first year at 13 tev." Internet: `https://atlas.cern/updates/atlas-news/atlas-completes-first-year-13-tev`, Dec. 2015. [2017-04-20].

[10] "Cosmic background explorer." Internet: `https://lambda.gsfc.nasa.gov/product/cobe/`, Jun. 2008. [2017-04-25].

[11] "Wilkinson microwave anisotropy probe." Internet: `https://map.gsfc.nasa.gov/`, Jul. 2013. [2017-04-25].

[12] J. H. Reif and S. R. Tate, "The complexity of n-body simulation," in *20TH ANNUAL COLLOQUIUM ON AUTOMATA, LANGUAGES AND PROGRAMMING (ICALP'93*, pp. 162–176, 1993.

[13] J. Read, "Dark matter." Internet: https://indico.lucas.lu.se/event/399/contribution/0/material/3/0.pdf. Lecture notes, University of Surrey, [2017-05-02].

[14] F. Kahlhoefer, "Review of lhc dark matter searches," *International Journal of Modern Physics*, vol. A32, 2017.

[15] C. D. Oliver Buchmueller and L.-T. Wang, "Search for dark matter at colliders," *Nature Physics*, vol. 13, p. 217–223, Mar. 2017.

[16] G. Aad *et al.*, "The atlas experiment at the cern large hadron collider," *Journal of Instrumentation*, vol. 3, no. 08, 2008.

[17] D. Abercrombie *et al.*, "Dark Matter Benchmark Models for Early LHC Run-2 Searches: Report of the ATLAS/CMS Dark Matter Forum," 2015.

[18] "Atlas explores the dark side of matter." Internet: http://cerncourier.com/cws/article/cern/65017. [2017-03-12].

[19] C. Doglioni and A. Boveia, "Monox.pdf." Internet: https://commons.wikimedia.org/wiki/File:MonoX.pdf, Sep. 2016. [2017-04-26].

[20] T. Sjöstrand *et al.*, "An introduction to pythia 8.2," 2014.

[21] T. Sjostrand, "Monte Carlo Tools," in *Proceedings, 65th Scottish Universities Summer School in Physics: LHC Physics (SUSSP65)*, pp. 309–339, Aug. 2009.

[22] "Summary plots from the atlas exotic physics group." Internet: https://atlas.web.cern.ch/Atlas/GROUPS/PHYSICS/CombinedSummaryPlots/EXOTICS/index.html#ATLASDarkMatterSummary,https://cds.cern.ch/record/2208044, Mar. 2017. [2017-04-27].

[23] A. Boveia *et al.*, "Atlas dm summary plots." Internet: https://indico.cern.ch/event/563066/contributions/2305848/attachments/1338837/2015261/20160919_DMWG_DMSummaryPlots.pdf. [2017-04-27].

[24] P. Tunney, M. Fairborn, and F. Kahlhoefer, "Relic density in simplified models of dark matter - the axial vector case." Internet: https://indico.cern.ch/event/563066/contributions/2306998/attachments/1339661/2016859/Tunney_DMWG_MadDM.pdf, Sep. 2016. [2017-04-27].

[25] S. Agostinelli *et al.*, "GEANT4: A Simulation toolkit," *Nucl. Instrum. Meth.*, vol. A506, pp. 250–303, 2003.

[26] F. Krauss, "Detector & statistics in a nutshell." Internet: https://www.ippp.dur.ac.uk/~krauss/Lectures/QuarksLeptons/Basics/Det_1.html. Lecture notes, University of Durham, Durham, UK, [2017-05-03].

[27] "Search for new phenomena in dijet mass and angular distributions from pp collisions at $\sqrt{s}$ = 13 tev with the atlas detector." Internet https://atlas.web.cern.ch/Atlas/GROUPS/PHYSICS/PAPERS/EXOT-2015-02/, Dec. 2015. [2017-05-03].

[28] G. Aad *et al.*, "Search for new phenomena in dijet mass and angular distributions from *pp* collisions at $\sqrt{s} = 13$ TeV with the ATLAS detector," *Phys. Lett.*, vol. B754, pp. 302–322, 2016.

[29] C.-Y. Wong, "Pseudorapidity variable," in *Introduction to High-Energy Heavy-Ion Collisions*, ch. 2.4, p. 24, WORLD SCIENTIFIC, 2011.

[30] D. Gillberg, "Search for new physics in the dijet and photon+jet angular and mass distributions with the atlas detector." Internet: https://indico.cern.ch/event/181298/contributions/309302/. [2017-05-01].

[31] J. E. Gaiser, *Charmonium Spectroscopy from Radiative Decays of the J/Psi and Psi'*. PhD thesis, Stanford University, Stanford, California 94305, Aug. 1982. p. 178.

[32] I. Dinov, "Introduction to statistical methods for the life and health sciences." Internet: http://www.stat.ucla.edu/~dinov/courses_students.dir/06/Fall/STAT13.1.dir/STAT13_notes.dir/lecture10.pdf. Lecture notes, University of California, Los Angeles, USA, [2017-05-03].